Surface & Coatings Technology 398 (2020) 126093

Contents lists available at ScienceDirect

Surface & Coatings Technology

journal homepage: www.elsevier.com/locate/surfcoat

High-temperature oxidation behavior of CuAlNiCrFe high-entropy alloy bond coats deposited using high-speed laser cladding process

Qing-Long Xu, Yu Zhang, Sen-Hui Liu, Chang-Jiu Li, Cheng-Xin Li*

State Key Laboratory for Mechanical Behavior of Materials, School of Materials Science and Engineering, Xi'an Jiaotong University, Xi'an, Shaanxi 710049, China

ARTICLE INFO

Keywords:
High-entropy alloy
High-speed laser cladding
Oxidation behavior
CuAlNiCrFe
Thermal barrier coating
Bond coat

ABSTRACT

A promising new bond coat using CuAlNiCrFe high-entropy alloy was proposed in this paper. The difference in pre-oxidation conditions between the traditional thermal-sprayed MCrAlY bond coat and CuAlNiCrFe high-entropy alloy bond coat deposited using high-speed laser cladding was investigated. The result confirmed that the CuAlNiCrFe high-entropy alloy bond coat deposited using high-speed laser cladding can complete the pre-oxidation faster and form a continuous α-Al_2O_3 thermally grown oxide (TGO), which shortens the initial oxidation stage, thereby avoiding the formation of other oxides and spinel structures. In the subsequent isothermal oxidation process, the block-like structure of the high-speed laser cladding layer and the sluggish diffusion effect of the high-entropy alloy work together to ensure the slow and continuous supply of aluminum element to TGO layer and obtain a low growth rate. Also, the diffusion between the bonding layer and the substrate is controlled at a low level, and the new CuAlNiCrFe bond coat exhibits excellent oxidation and diffusion resistance. With the consumption of aluminum, the phase structure of the high-entropy alloy bond coat changed from BCC to FCC, but it still maintained a stable simple solid solution structure.

1. Introduction

Thermal barrier coatings (TBCs) are an important thermal protection system for propulsion and power generation that are composed of a top ceramic layer and a bond coat between the ceramic layer and substrate [1]. The TBCs utilize the high-temperature resistance of ceramics, and they reduce the operating temperature of the metal parts, extend the service life and improve the working efficiency of an engine [2]. Currently, the advanced TBCs are typically fabricated on the surface of a nickel or cobalt based super-alloy substrate. The entire structure is constituted using a Y_2O_3 stabilized ZrO_2 (YSZ) top coat, thermally grown oxide (TGO) layer, and an MCrAlY (where M is Ni, Co, or a mixture of Ni and Co) bond coat. Each layer has its own role: the top coat provides thermal insulation, while the thermally grown oxide (TGO), from the bond coat thermal growth, helps in preventing further oxidation and diffusion. The bond coat is critical to avoid the direct contact between the top ceramic layer and substrate, thereby acting as a connector and protector. Essentially, it is the most significant component of the TBC system to influence durability using the TGO layer formed as the bond coat oxidizes [3]. A traditional MCrAlY bond coat material usually chooses Ni, Co or Ni + Co as the matrix element, which mainly determines the thermal corrosion resistance; when the percentage of Co is between 20% ~ 26%, the MCrAlY coat combined with Ni can have better corrosion resistance and the best ductile property. Al, Cr determine the oxidation resistance property of the coat. During the high-temperature oxidation process for a long duration, a layer of uniform and dense aluminum oxide layer is formed on the interface which resists further oxidation of the bond coat [3,4]. Moreover, the ratio of Al to Cr is important for alumina production; aluminum oxide is formed when the ratio is lower than 4 [5]. Some reports have shown that 0.3% ~ 1.0% addition of Y can improve the adhesion between the alumina and substrate. Further, the thermal shock performance and oxidation resistance of the coating can also increase.

Typically, each interface damage may lead to the failure of the entire TBC system. However, through a number of experiments, the researchers have discovered that the interface between the top ceramic coat and the bond coat is the weakest part, the spallation of YSZ usually appears nearby the TGO layer. The TGO layer is mainly alumina. As the oxidation process proceeds further, aluminum is consumed continuously, resulting in insufficient supply of aluminum and appearance of spinel-type structures and other oxides. This is harmful for the service life of the TBC [6]. The stress increases sharply, leading to the weakening of the bond between the top ceramic layer and the bond coat, and finally the ceramic layer falls off and the TBC system fails [7].

Abbreviations: TBCs, thermal barrier coatings; TGO, thermal growth oxide; HEA, high-entropy alloys; SEM, scanning electron microscopy; XRD, X-ray diffraction

* Corresponding author.
E-mail address: licx@mail.xjtu.edu.cn (C.-X. Li).

https://doi.org/10.1016/j.surfcoat.2020.126093
Received 21 April 2020; Received in revised form 10 June 2020; Accepted 20 June 2020
Available online 22 June 2020
0257-8972/

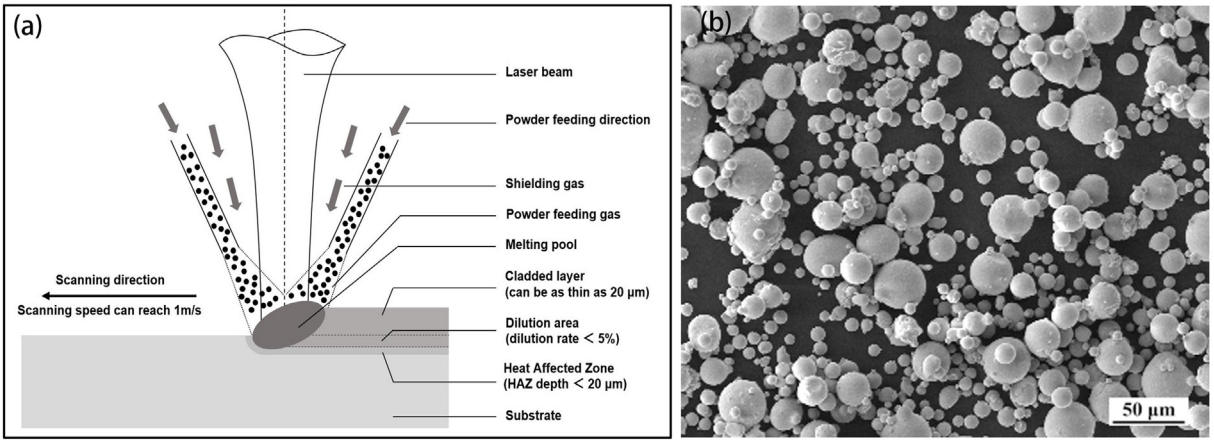

Fig. 1. (a) Schematic diagram of high-speed laser cladding process compared to traditional laser cladding and (b) the morphology of CuAlNiCrFe high-entropy alloy powder.

Since the appearance and growth of TGO is inevitable, it is necessary to regulate the composition and structure of the bond coat, so as to control the growth rate of TGO [8]. At present, spraying is the primary method of preparation of the bond coat; the atmospheric plasma spraying (APS), flame spraying (FS), and arc spraying (AS) methods usually have poor oxidation resistance because of the presence of more pores and oxides in the as-deposited samples [9,10]. Comparatively, electron beam physical vapor deposition (EB-PVD), high velocity oxygen fuel spraying (HVOF), low pressure plasma spraying (LPPS) or vacuum plasma spraying (VPS), multi-arc ion plating (MAIP), and cold gas dynamic spraying (CGDS) can make more dense samples with less oxidation; the growth rate of the TGO layer of these coatings is slower [11–15]. After the preparation of the bond coat, post-treatment is necessary for the improvement of the bond coat properties to make it effective enough [1,16]. Presently, the most effective treatment is pre-oxidation. This is a diffusion treatment carried out in a furnace filled with Ar, and the low-oxygen partial pressure ensures that only one layer of dense α-alumina is generated on the surface of the bond coat during post-treatment with no other oxides. Therefore, alumina can continue to grow and reach a certain thickness in the following atmospheric oxidation process; thus, the oxide layer formed by pre-oxidation plays a protective role for the matrix and has a low TGO growth rate and long service life [17].

Both terrestrial gas turbines and aviation gas turbines have increasingly high requirements for operating temperature due to the high demand for power. As a very important aspect of the thermal barrier coating system, the metal bond coat must further improve the high-temperature oxidation resistance to increase the operating temperature of the thermal barrier coating system. The high-entropy alloy (HEA), a new material system that has emerged in the recent years, with single-phase solid solution structure, has far more thermal stability and high-temperature oxidation resistance than the traditional alloys [18,19]. Through the composition design of the high-entropy alloy, the bond coat surface can be controlled to generate a continuous and dense oxide layer. The oxidation behavior of FeCoNiCrAl, FeCoNiCrMn, and FeCoNiCrSi HEAs was investigated at 900 °C for 48 h. Among them, FeCoNiCrAl showed good oxidation resistance due to the formation of the oxide layer consisting of Al_2O_3 and $FeA_{l2}O_4$ with a thickness of 2.15 ± 0.15 μm [20–22]. In summary, the high-entropy alloy for bond coat has higher thermal stability and the sluggish diffusion effect reduces the oxidation consumption rate of Al and Cr elements in the bond coat. Meanwhile, the degradation due to the diffusion of elements between the bond coat and the metal substrate can also be alleviated. High-entropy alloy is a promising material for application in bond coating [23]. Further, the lamellar bond coat structure formed using plasma-spraying technology is not conducive to the continuous diffusion of aluminum element, and it is not easy to control the proportion of elements in the vapor deposition of multiple components technology. Hence, high-entropy alloy with high thermal properties and an effective control on TGO thickness poses a challenge for the metallurgical bond between the thin bond coat and metal substrate.

Traditional laser cladding technology can obtain a cladding layer combined with the metal substrate metallurgically, but the thickness of the traditional laser cladding layer is usually more than 500 μm, and the thermal impact on the substrate is another problem that needs to be addressed [24,25]. The ultra-high-speed laser cladding technology was jointly developed by Fraunhofer ILT and RWTH aachen university (Aachen) in 2017 which solved the bottleneck problem of low coating processing efficiency and thus provided the possibility for large-scale applications of laser cladding technology [26]. The coating surface prepared by ultra-high-speed laser cladding was well formed, with dense internal structure, no defects, high bonding strength with the matrix, excellent mechanical properties and corrosion resistance. This could meet the needs of surface strengthening and functionalization of most high-end equipment. As an extension and development of spraying technology, ultra-high-speed laser cladding technology greatly improved the bonding strength between the coating and substrate. At the same time, it overcame the shortcomings of the traditional laser cladding layer, which was extremely thick and the heat input to the substrate was large just shown in Fig. 1(a). The high laser cladding rate and the fact that most of the laser energy was applied to the powder made it possible to achieve a thin coat with a thickness of less than 50 μm and with a dilution rate as low as 1%. Even the thermal effect of laser cladding on matrix could be neglected. In addition, ultra-high-speed laser cladding had the advantages of high cooling rate and easy regulation of laser cladding powder composition, which helped in obtaining ultra-fine coating grains and precise coating composition control.

In this study, a thin and metallurgically bonded high-entropy alloy material bond coat deposited using ultra-high-speed laser cladding method was put forward to achieve the thermal stability and diffusion resistance of the high entropy [27], and utilize the advantages of ultra-high-speed laser cladding at the same time. For example, fast preparation, superfine grains, greater solid solubility, the as-cast structure similar to the substrate and the metallurgical bonding with substrate. The experiment showed that the growth of the TGO layer on the bond coat was within a reasonable range. Meanwhile, the new type of bond coat revealed amazing diffusion resistance and good phase stability, no spinel structures or other oxides were present during the entire oxidation process. Later, the CuAlNiCrFe high-entropy alloy bond coat deposited using high-speed laser cladding was examined in a complete TBC system. They exhibited long high-temperature oxidation life.

2. Experimental procedures

2.1. Experimental materials

Nickel-based superalloy Inconel718 (φ 25.4 mm × 3 mm) was used as the substrate. The nominal composition (wt%) of this superalloy was 51.96Ni-17.98Cr-3.07Mo-0.95Ti-4.82Nb-0.45Al-Bal.Fe. Prior to the laser cladding, the substrate was first polished with a file to expose the fresh metal, and then ultrasonically cleaned with acetone to remove residual impurities from the surface. Commercial CuAlNiCrFe powder (Zhonghangmaite, China) with a nominal composition (wt%) of 22.78Cu-10.23Al-23.63Ni-19.98Cr-22.02Fe was used as the feedstock powder. The CuAlNiCrFe powder particles were spherical in shape, and the particle size distribution was from 45 to 105 μm. A commercial CoNiCrAlY (Amdry 9951, Oerlikon Metco, Switzerland) with a nominal composition (wt%) of Co-23.0Ni-17.0Cr-13.0Al-0.5Y was used to prepare a typical thermal spray coating by HVOF method as a comparison to show the difference of pre-oxidation mechanism between traditional thermal spray MCrAlY bond coat and high-entropy alloy bond coat using high-speed laser cladding. The surface morphology of CuAlNCrFe powders are shown in Fig. 1(b).

2.2. Coating deposition

The CuAlNiCrFe bond coat with a thickness of about 200 μm was cladded on the surface of the Inconel718 substrate using a combination of commercial laser equipment and self-made mobile platform. The high-speed laser cladding parameters are listed in Table 1. For the laser cladding, high purity argon (Ar ≥ 99.999%) was used as the protecting gas and powder feeder gas. A 200 μm thick traditional NiCoCrAlY bond coat was sprayed by HVOF as a contrast showing the pre-oxidation characteristic of thermal spray, Table 2 shows the spraying parameters of HVOF.

2.3. Pre-oxidation treatment and isothermal oxidation test

The as-cladded CuAlNiCrFe bond coats were subjected to a controlled atmosphere pre-oxidation treatment with Ar gas flow (1 h, 2 h and 4 h at 1050 °C, P(Ar) ≥ 1×10^5Pa, P(O_2) < 0.001 Pa) in an industrial tube furnace. The reason for employing such heat-treatment conditions is that the heat treatment controls the oxygen partial pressure and a layer of alumina is formed. Later, isothermal oxidation tests were employed at 1100 °C for 4 h, 25 h, and 100 h to characterize the oxidation resistance properties of the bond coats [28].

To further verify the performance of this kind of HEA bond coat, a commercial 8YSZ splats were deposited on the bond coat by atmospheric plasma spraying (APS, 80 kW class, Jiujiang China) at a plasma arc power of 42 kW (60 V, 700 A). During plasma spraying, the anode nozzle of an internal diameter of 5.5 mm and a length of 33 mm was used. Argon at a pressure of 0.9 MPa and a flow rate of 45 L/min was used as primary gas. Hydrogen at a pressure of 0.4 MPa and a flow rate of 7 L/min was used as secondary gas. Nitrogen was used as the powder carrier gas with a pressure of 0.4 MPa and a flow rate of 7 L/min. The spray powders were injected radially into the anode nozzle by an internal injector 12 mm away from the exit of the anode nozzle. The spray distance was fixed to 80 mm. To show its superior performance as compared with that of the traditional TBC systems, it was directly exposed to a heat environment at 1100 °C for 50 h.

Table 1
High-speed laser cladding parameters.

Power	2.0 kW
Working distance	15 mm
Carrier/inert gas	Ar
Gas flow rate	6 L/min
Powder feeder speed	0.3 g/s
Scanning speed	260 mm/s
Overlap rate	80%

Table 2
Spraying parameters of HVOF.

Oxygen pressure(MPa)	1.0
Air pressure(MPa)	0.7
Propane gas pressure(MPa)	0.8
Powder feeder gas pressure(MPa)	1.1
Spraying distance(mm)	225

2.4. Microstructural characterization

A field emission scanning electron microscope (SEM, MIR 3 LMH, TESCAN, Czech Republic) equipped with EDS (Aztec, Oxford Instruments, United Kingdom) was employed to generate secondary electron (SE) images, backscattered electron (BSE) images, and EDS test data. Aqueous solution is used as an etchant to show the microstructure of the cladding layer. In order to ensure the accuracy of the surface TGO component detection in the pre-oxidation experiment, three areas are randomly selected for detection to display the standard deviation of the EDS test data. In addition to this, X-ray diffraction (XRD, D8advance 3.0, Bruker, Germany) was performed to characterize the crystalline structure of the TGO layer. The analysis parameter of the samples are: the 2θ range is 10–90° and the step size is 0.1°. Further, in order to protect the TGO layer from being damaged during grinding, a layer of Ni was deposited by electroplating.

3. Result and discussion

3.1. Dense and uniform high-speed laser cladding layer

High-speed laser cladding technology ensures that the laser energy predominantly acted on the powders by adjusting the relative positions of the focus point of the laser, focus point of the powders flow, and the substrate. The high-speed laser cladding technology has lesser influence on the substrate i.e. less melting of the substrate and lower dilution of the elements as compared to that of the traditional laser cladding technology, which has a high dilution rate. Fig. 2(a) and (b) shows the cross-sectional microstructure of the CuAlNiCrFe high-entropy alloy bond coat after the initial high-speed laser cladding. The BSE image confirms the existence of an evident interface between the cladding layer and matrix. The EDS line scanning in Fig. 2(c) shows that the element transition zone is only a few dozen microns wide and the effect of laser cladding on the substrate was small. These SEM results indicate that a dense and uniform laser cladding bond coat can be prepared without any cracks using the high-speed laser cladding. Moreover, Fig. 2 (d), (e) and (f) show that the microstructure of the cladding layer is mainly columnar crystals and a small amount of dendrites and equiaxed crystals. The growth direction of the columnar crystals is related to the direction of heat dissipation and the formation of a small amount of equiaxed crystals near the surface layer is due to the extremely fast surface cooling rate. Overall, the microstructure of the cladding layer is similar to the block material, and there is no layered structure similar to thermal spraying.

3.2. The pre-oxidation behavior of traditional MCrAlY bond coat deposited by HVOF

The traditional NiCoCrAlY bond coat prepared using HVOF was selected as an example of thermal spraying to show the pre-oxidation difference between the traditional thermal spray MCrAlY bond coat and new high-entropy alloy bond coat using high-speed laser cladding. The conventional bonding coats usually require 4–8 h to complete the pre-oxidation process and a summary of the pre-oxidation parameters of

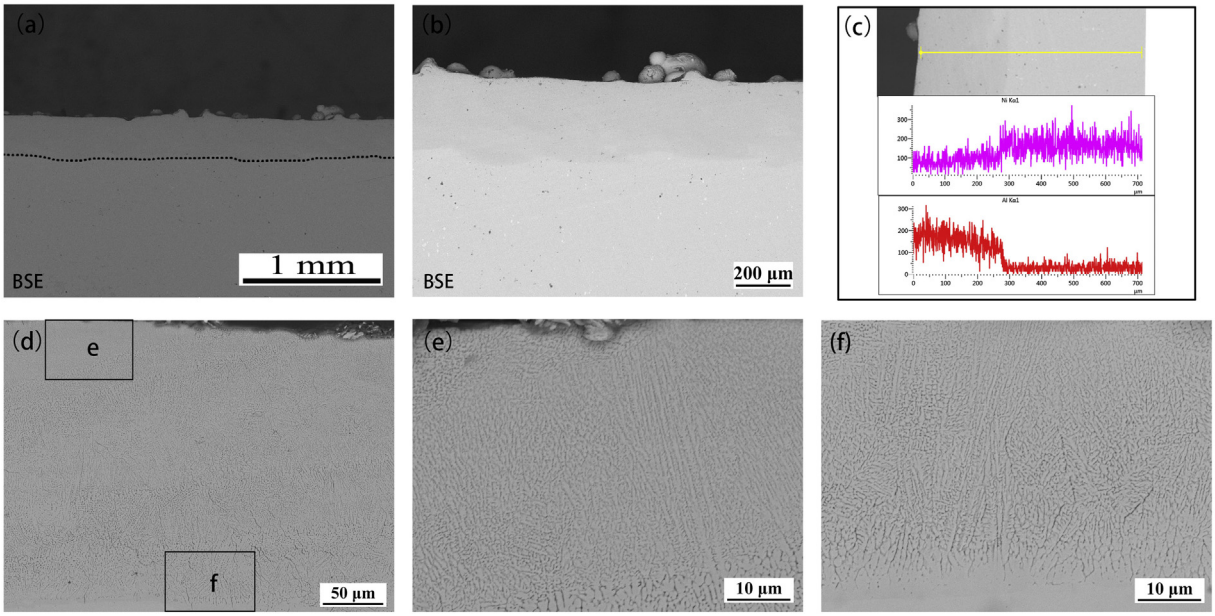

Fig. 2. The cross-section morphology of continuous and dense CuAlNiCrFe laser cladding layer in a large (a) and usual scale (b); (c) EDS line scanning of Ni, Al elements vertically down from the top of the coating; (d) the microstructure of the whole CuAlNiCrFe laser cladding layer; (e) and (f) show the enlarged microstructure in (d).

Table 3
Summary of the pre-oxidation parameters of MCrAlY coatings prepared by different thermal spraying processes.

Material	Preparation	Pre-oxidation parameters	Ref
CoNiCrAlY	APS	1100 °C for 10 h in the presence of Ar	[1]
CoNiCrAlY	EB-PVD	1050 °C for 4 h in an Ar flow	[29]
CoCrAlY	HVOF	1050 °C for 4 h in an Ar flow 1050 °C for 4 h + 950 °C for 10 h 1050 °C for 4 h + 1000 °C for 10 h	[30]
NiCoCrAlY	EB-PVD	1050 °C for 4 h in controlled atmosphere	[31]
CoNiCrAlY	APS	1100 °C for 4 h and 10 h in vacuum	[32]
CoNiCrAlY	VPS	1050 °C for 4 h in an Ar flow	[33]

MCrAlY coatings prepared by different thermal spraying processes is shown in Table 3 [1,29–33]. The bond coat needs time to complete the initial surface oxidation nucleation process and form a protective and stable oxidation film according to the Wagner's selective oxidation theory [34]. A 2 h, 4 h and an 8 h pre-oxidation experiment showed the transformation process of the surface morphology and the surface components. We can directly see the process of generation of Al_2O_3 from 2 h to 8 h of the pre-oxidation process in Fig. 3(a)–(c). When the samples are under 1050 °C for 4 h, aluminum oxide is formed in some areas of the surface, but most of the areas are not completely oxidized. This indicates that the pre-oxidation process needs an additional 4 h to form a protective oxide film on the surface of the bonding layer. The upper surface of the bond coating under the 8 h pre-oxidation condition is completely coated with alumina, The EDS map scanning result in Table 4 has affirmed this point. Of course, pre-oxidation also helps to improve the performance of the MCrAlY coating deposited by HVOF, such as density, hardness and bond strength, and here we mainly focus on the formation and evolution of the TGO layer [35,36]. In addition, some things need to be explained clearly that a small amount of other elements appear in the EDS map scanning results and this is because the penetration depth of the electrons emitted by the scanning electron microscope is about a few microns, which is greater than the thickness of the pre-oxidized surface alumina. Some elements in the bond coat can be detected, but it can still be determined that alumina is indeed formed on the surface after pre-oxidation. The cross-section image after plating nickel on the upper surface of the sample in Fig. 3(d) also confirmed this and the map scanning results indicated the composition of TGO is O and Al elements, which further confirmed that the alumina film was formed. In addition, the lamellar interfacial oxide between the splats inside the coating was observed. There are two types of lamellar interfacial oxide, one is oxide inclusions, interaction of the in-flight hot powder particles with their surrounding environment leads to formation of oxide inclusions between the splats [37].The other is due to the existence of pores in thermal spray coat, oxygen enters the interior of the coating through the pores, and selective oxidation occurs under low oxygen partial pressure to form oxides.

3.3. A new pre-oxidation behavior exhibited by CuAlNiCrFe bond coat deposited using high-speed laser cladding

Different from the traditional MCrAlY bond layer, the high-entropy alloy bond layer formed using high-speed laser cladding show completely different characteristics of pre-oxidation as seen in Fig. 4(a). A thin film of alumina is formed in a shorter time for a CuAlNiCrFe HEA as compared to that for a traditional one [38] and the EDS test result of CuAlNiCrFe bond coat surface after pre-oxidation for 1 h in Table 5 proves the oxide composition. A continuous and dense large-area alumina covers the surface of the bond coat in 1 h, 2 h and 4 h shown in Fig. 4(b)-(e) which act as a protective layer. This can be explained as Fig. 5. The bulk-like structure of high-entropy alloy bond layer using high-speed laser cladding is different from the lamellar structure of the traditional MCrAlY [1,39,40]. The lamellar interfacial block effect of the unbound interface, surface oxide and partial metallurgical bonding due to the thermal spray technology leads to a slow diffusion of aluminum in MCrAlY coat. When the coat is exposed to a high temperature-atmospheric environment, the oxidizable elements diffuse into the coat surface. The Al element content in a single splat is not enough to form a continuous layer of alumina oxide on the surface of the bond coat and the lamellar interface hinders the element diffusion from the nearby splats. Therefore, unpre-oxidized MCrAlY coatings sometimes produce a spinel-type structure at high temperatures [1]. However, the high-entropy alloy bond coat using high-speed laser cladding shows a continuous structure resembling a metal block and complete metallurgical bonding with the substrate. This helps in providing continuous element supply during the whole oxidation process to prevent

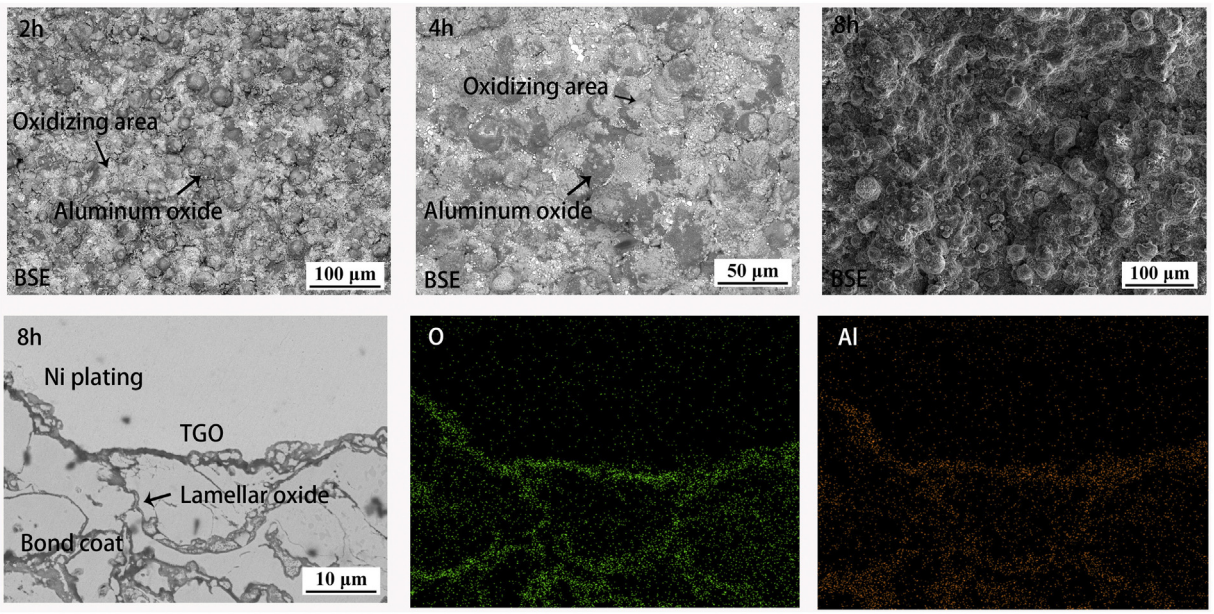

Fig. 3. The surface morphology and one of the cross section EDS mapping under different time pre-oxidation conditions; (a), (b), and (c) show the surface morphology of the conventional MCrAlY bond coat deposited by HVOF after 2, 4, and 8 h of oxidation under the condition of 1050 °C and controlled oxygen partial pressure P(O_2) < 0.001 Pa; (d) shows the cross section BSE image and the EDS mapping of Al, O elements after 8 h oxidation under the above pre-oxidation conditions.

Table 4
The EDS test result of MCrAlY bond coat surface after pre-oxidation for 8 h.

Element	O	Al	Cr	Mn	Fe	Co	Ni
At.%	55.7 ± 1.1	20.7 ± 1	9.3 ± 1.5	2.3 ± 0.3	2.6 ± 0.1	5 ± 0.3	4.3 ± 1.1

the formation of some other oxides or spinel-type structure. Of course, in the initial stages of oxidation, the diffusion of aluminum is easy and a protective alumina layer can be formed on the surface quickly. Note that, although the high-entropy alloy deposited using high-speed laser cladding can form an alumina film on the surface of the bond coat faster than a traditional thermal sprayed MCrAlY coat, previous reports have shown that the diffusion coefficient of aluminum element in high-entropy alloy is much lower than that in the traditional Ni-Cr-Fe alloy [41–45]. A larger lattice potential energy fluctuation in the high-entropy alloy leads to higher normalized activation energies and a lower diffusion rate. Logarithm of diffusion coefficient ($m^2 \cdot s^{-1}$) of aluminum element in high-entropy alloy is approximately −14, and that in the traditional Ni-Cr-Fe alloy is approximately −10 or − 11.The extremely low diffusion coefficient of high-entropy alloy due to the lattice distortion guarantees the slow diffusion and consumption of Al element. An approximately equal inter-diffusion of Fe and Cr happens between the CuAlNiCrFe coat and the substrate because the Cr and Fe content in them are similar. The pre-oxidation time was so short that we utilized just one hour or less to complete the pre-oxidation process.

However, it cannot be said that the aluminum oxide growth was rapid because the entire oxidation process includes the initial oxidation stage and stable oxidation stage. The complete oxidation film was not formed in the initial oxidation stage as the high-entropy alloy bonding layer greatly shortened this stage. After the formation of the protective alumina film, the oxidation rate was governed by the Al and O ion diffusion in the thermal growth oxide (TGO) layer and it was very low [46,47]. The later TGO growth kinetic curves can be used to help prove this point.

3.4. Isothermal oxidation behavior of high-entropy alloy bond coat deposited using high-speed laser cladding

An isothermal oxidation test was carried out after the pre-oxidation treatment at 1100 °C for different times to verify the oxidation resistance. A layer of electroplated nickel was deposited on top of the TGO to protect the TGO during samples preparation. The alumina layer formed on the surface of the bond coat during the pre-oxidation process continued to grow. When the oxidation time was increased from 4 h to 100 h, the thickness of the pure alumina-TGO layer increased from 0.89 μm to 3.2 μm due to the diffusion of Al element from the bond coat to the top surface in Fig. 6(a), (b) and (c). The undulation was observed in Fig. 6(b) and there may be more than one reason [48,49]. The phase transformation of bond coat and the residual stress caused by the growth of TGO may cause this phenomenon [50,51]. The HEA bond coat using high-speed laser cladding exhibits a medium TGO growth rate that the oxidation rate constant is 0.264 μm/$h^{1/2}$. The curves in Fig. 7(a), (b), (c) and (d) representing the difference in element concentration in the bond coat during the growth of TGO was provided to describe the element diffusion between 0 h(as-cladded state), 4 h, 25 h and 100 h of oxidation and the bond-coat/substrate interface is shown in figures. The Al element diffuses in the direction of ceramic layer and substrate at the same time so the concentration of Al element gradually decreases, but is uniformly distributed throughout the cladding layer and the gradient of change is small. Fe and Cr are essentially unchanged in the bond coat due to their similar contents in the metal substrate. Ni and Cu have something different due to the significant concentration difference on both sides of the interface. At the beginning, the mass fraction of Cu in the coating is higher than that of Ni, but as the diffusion progresses, the content of Ni gradually exceeds the content of Cu. But if make a comparison over a long period of time between oxidation

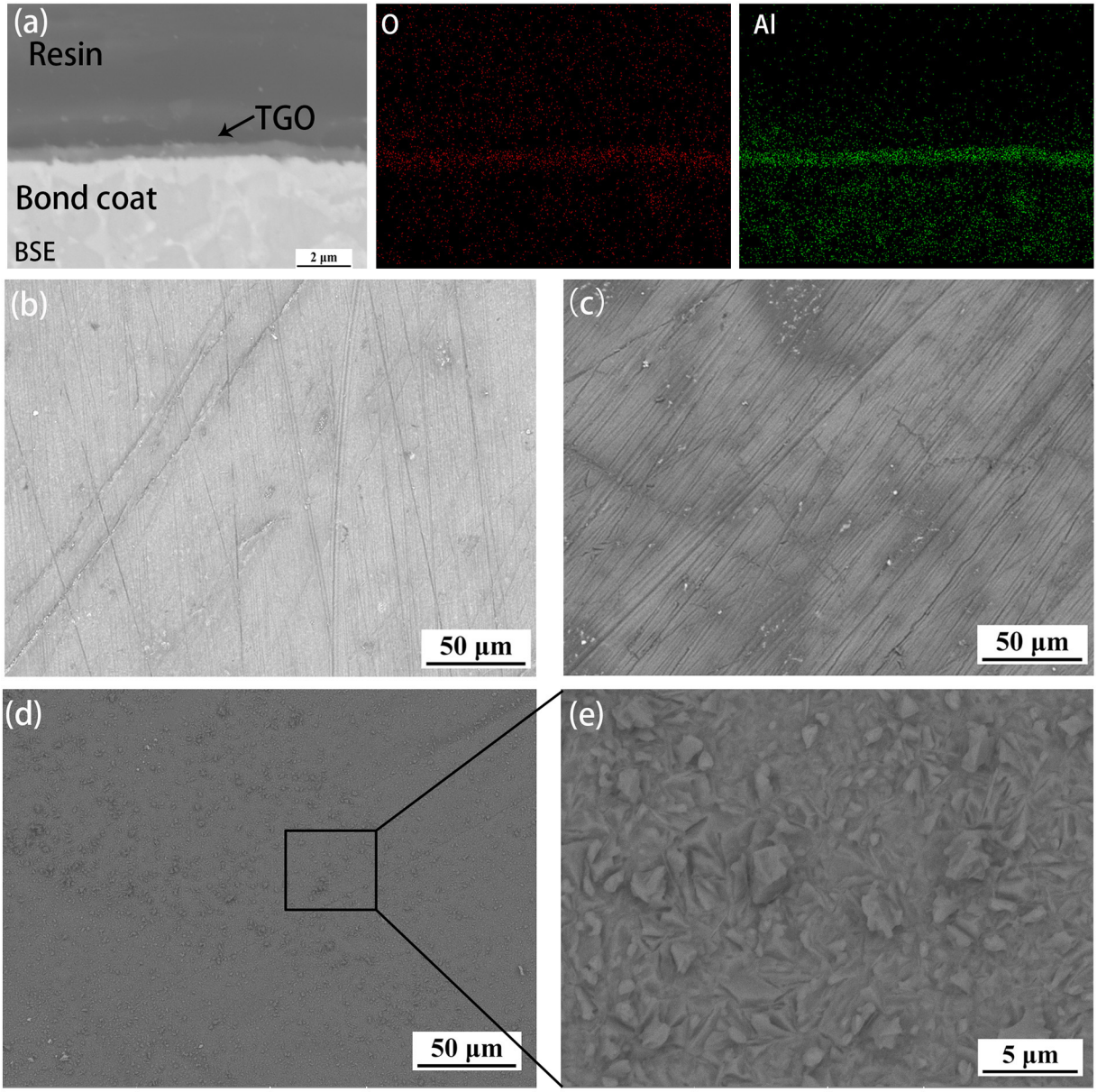

Fig. 4. The cross section and surface morphology of HEAs in different time pre-oxidation (a) show the BSE image and O,Al element EDS map scanning of CuAlNiCrFe bond coat after 1 h pre-oxidation at 1050 ˚C; (b), (c) and (d) show the BSE image of surface morphology of Cu AlNiCrFe bond coat after 1 h, 2 h and 4 h pre-oxidation at 1050 ˚C; (e) is a partially enlarged view of the (d).

for 25 h and 100 h, it can be seen that the mass fraction did not change more than 5%. Moreover, the concentration point of Al element under 1100 ˚C oxidation for 4 h is selected to roughly estimate the diffusion coefficient in Fig. 7(e). Since the calculation used is the Boltzman-Matona method, the concentration point is polynomial fitted by $y = -1.51962E - 4x^2 + 0.02077x + 9.52107$ and the Matona plane is calculated. The calculation results in Fig. 7(f) show that the diffusion coefficient of the Al element in HEA at 1100 ˚C is in the order of 10^{-14} and similar to that calculated in the previous literatures. At the same time, the diffusion coefficient of the Al element between the bond coat and the substrate is also controlled in the order of 10^{-14}, which is in a lower level compared with the MCrAlY literature [52] and indicates that the high-entropy alloy bonding layer has good resistance to diffusion. In general, the 1100 ˚C high-temperature oxidation test for 100 h has already proved the sluggish diffusion effect in high-entropy alloy and that the application of high-entropy alloy in the bonding layer can slow down the diffusion of elements in the bond TGO/bond-coat/substrate system. Besides, compared with the phase structure transformation from β-NiAl → γ'-Ni_3Al → γ–Ni when the aluminum in the traditional MCrAlY bonding layer is consumed, always maintaining a simple solid solution structure is another characteristic of HEA bond coat. The XRD mappings in Fig. 8(a) have exactly shown the excellent

Table 5
The EDS test result of CuAlNiCrFe bond coat surface after pre-oxidation for 1 h.

Element	O	Al	Cr	Fe	Ni	Cu
At.%	46.9 ± 1.1	28.2 ± 0.1	6.7 ± 0.5	6.1 ± 0.9	3.1 ± 0.8	9 ± 1.3

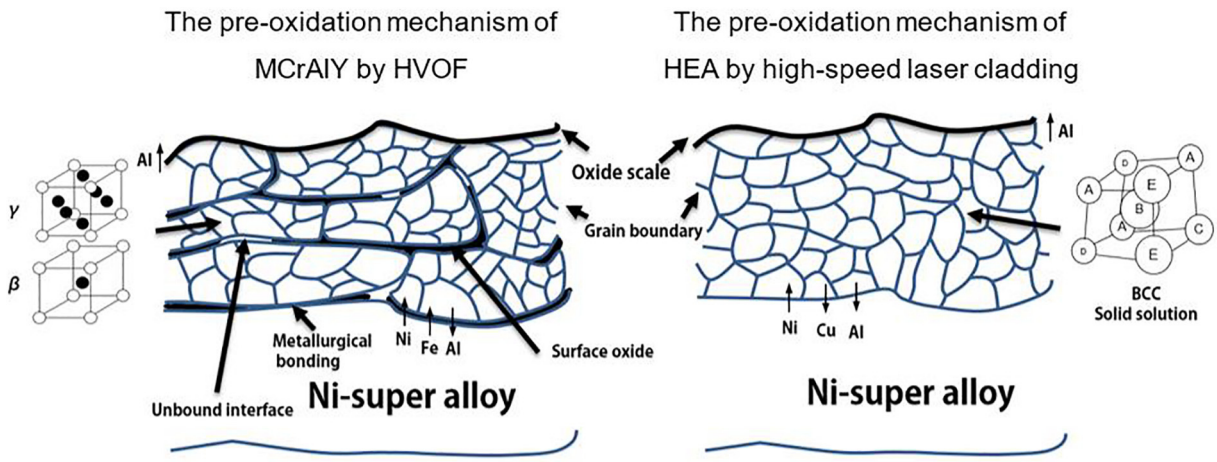

Fig. 5. The schematic of pre-oxidation difference between traditional MCrAlY by HVOF and HEA by high-speed laser cladding. The two kinds of lattice structures lead to different intrinsic diffusion coefficients of the material; The unbound interface, surface oxide and partial metallurgical bonding of the thermal sprayed lamellar structure lead to the blocking effect on the continuous diffusion of Al element.

phase stability that the bond coat is basically an FCC single-phase solid solution structure, which is characterized by good plasticity and strong deformation capacity after 100 h of oxidation [19]. The literature has shown that the Al content controls the phase structure in an AlxCoCrFeNi high-entropy alloy system [53]. Hence, the transformation in the phase structure can be considered as the result of the decrease in Al element content in combination with the change in Al element, as seen in the previous figure. The increment in Ni in the high-entropy alloy also helps in facilitating this shift. This phenomenon has previously appeared in the XRD data of high-entropy alloy coatings [23].

Isothermal oxidation at 1100 °C is considered to be a severe experimental condition. At this temperature, most of the bonding layer will be rapidly oxidized to form spinel and other structures, and can even cause the top ceramic layer to peel off. In literature, only a part of the bonding layer can be found to withstand a temperature of 1100 °C. It can be seen that the TGO growth rate of high-entropy alloy using ultra-high-speed laser cladding is better than that of the MCrAlY coating prepared using cold spraying or APS and is similar to that of the MCrAlY coating using HVOF or (Ni, Pt) Al coating prepared using EB-PVD [54–59]. It can be called as a promising method and material system for preparing the bond coat through the Fig. 8(b).

3.5. Isothermal oxidation test of TBC system with high-entropy alloy bond coating

In order to objectively evaluate the practical performance of the high-entropy alloy bond coat, a layer of YSZ ceramic coat was prepared on the surface of the bond coat after the pre-oxidation of the bond coat. To confirm the excellent performance of the new thermal barrier coating system, an oxidation experiment was performed under severe

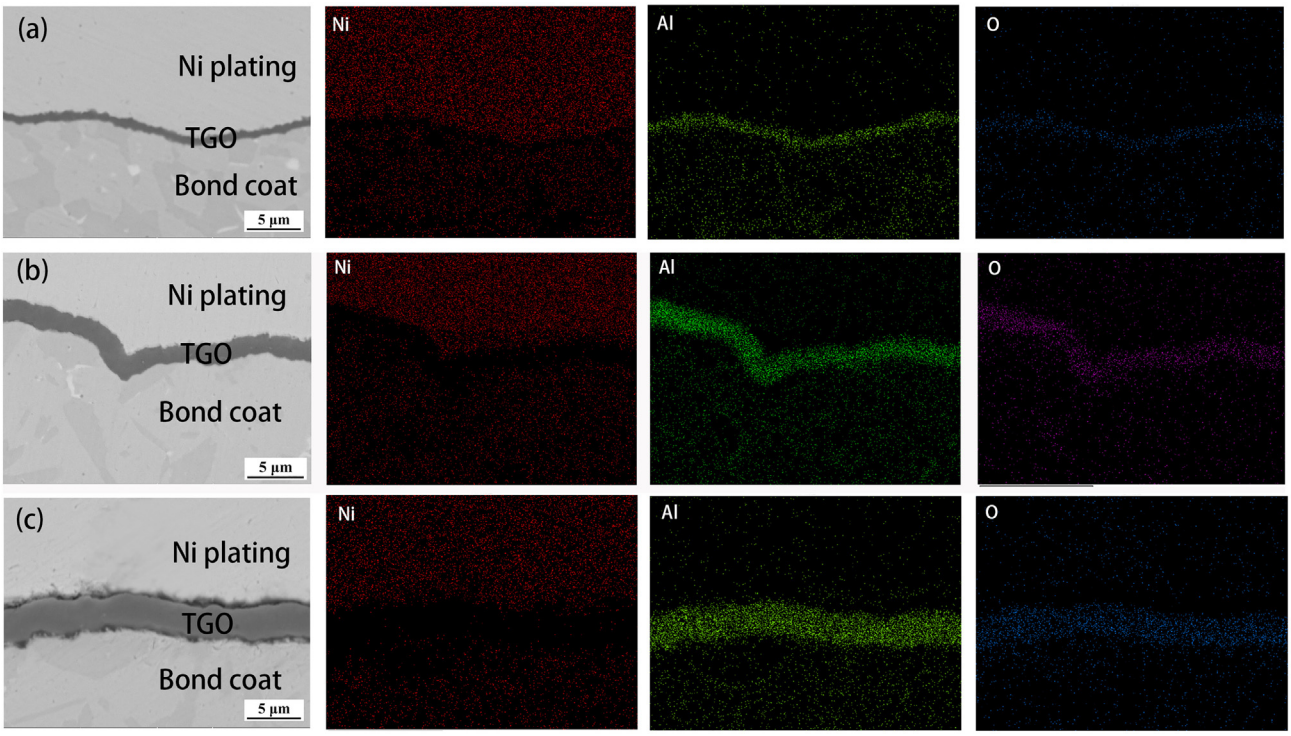

Fig. 6. The BSE cross-section image and Ni, Al, O element EDS mapping of CuAlNiCrFe bond coat after 4 h, 25 h and 100 h isothermal oxidation (a), (b), (c).

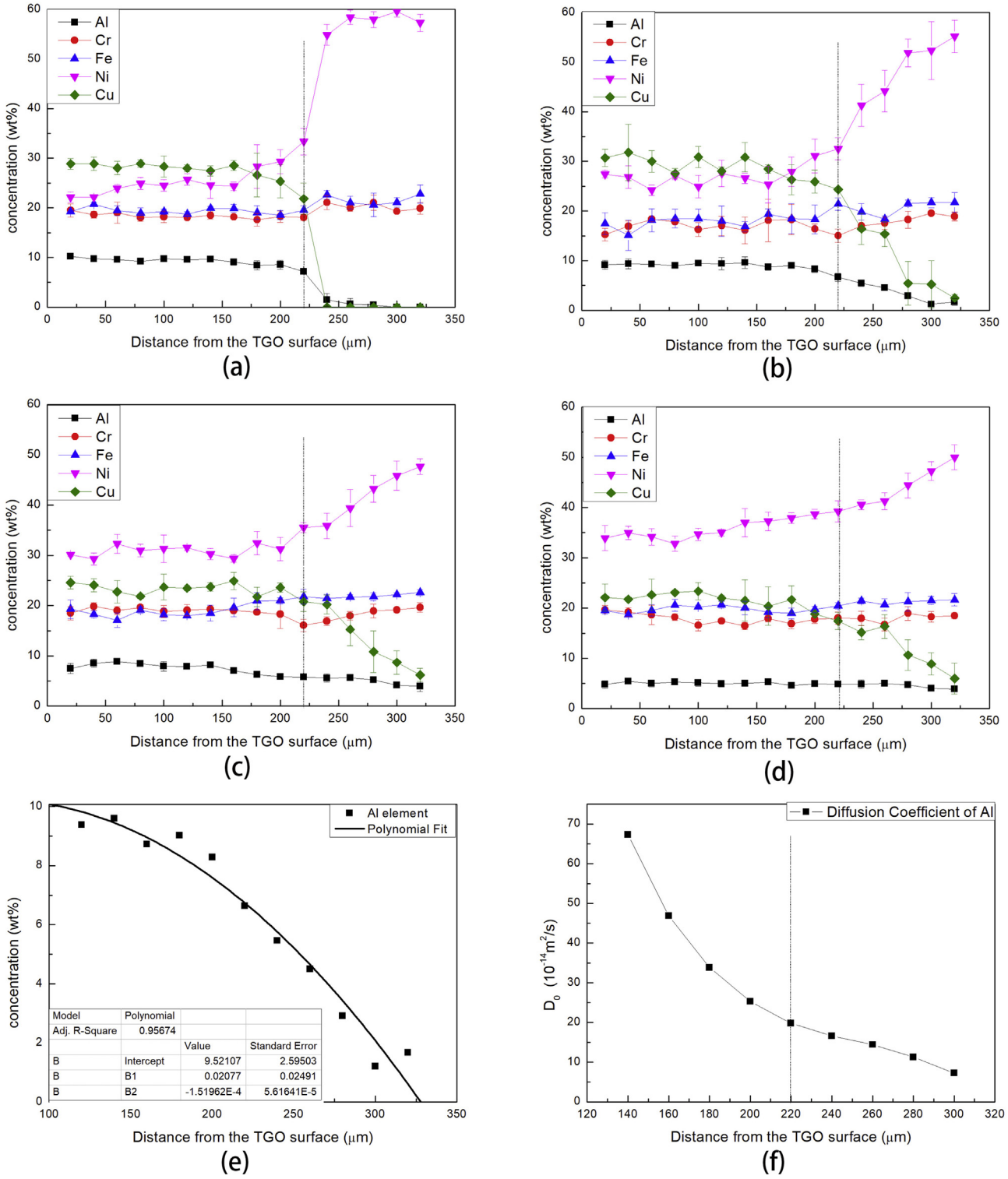

Fig. 7. The concentration curve from the top of the bond coat to the substrate after 0 h (as-cladded state), 4 h, 25 h and 100 h of oxidation (a), (b), (c), (d); (e) shows the concentration point and polynomial fitting curve of Al element near the interface after 4 h of 1100 °C oxidation in (b); (f) shows the diffusion coefficient of Al element calculated from the polynomial fitting curve in (e).

high temperature conditions at 1100 °C for 50 h. The experimental results after 50 h of oxidation in Fig. 9 exhibited excellent high temperature oxidation resistance in large areas. The top YSZ layer, the 3 μm-thick TGO layer on the surface of the bonding layer, the bonding layer and the substrate constituted an evident four-layer structure in the EDS map scanning. The pure alumina TGO layer acted as a protective film that blocked the external diffusion of metal elements and the internal diffusion of oxygen elements. The phase transformation in the bond coat from a BCC solid solution to an FCC solid solution was one of the reasons that the TGO layer was not as flat as before. Other reasons such as the residual stress could also be provided [60,61]. Element segregation was observed in the enlarged BSE image, but the XRD proved that the second phase did not appear, and the single-phase solid solution state of the high-entropy alloy was still maintained. It can be

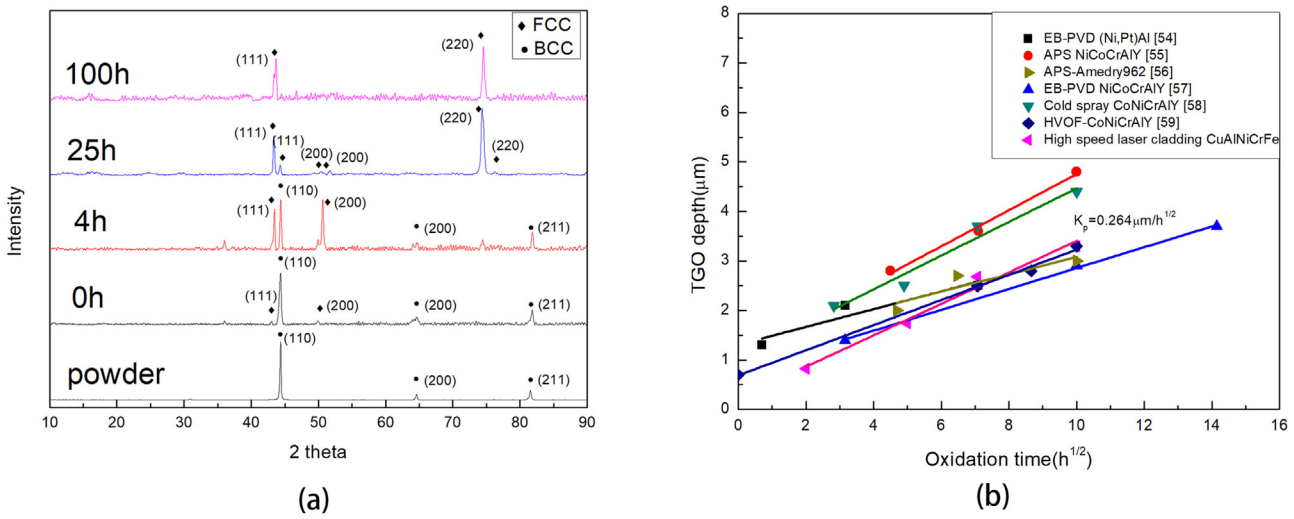

Fig. 8. (a) the XRD patterns of CuAlNiCrFe after different durations of oxidation.
and (b) The TGO growth kinetic curves of different materials in different processes at 1100 °C isothermal oxidation [54–59].

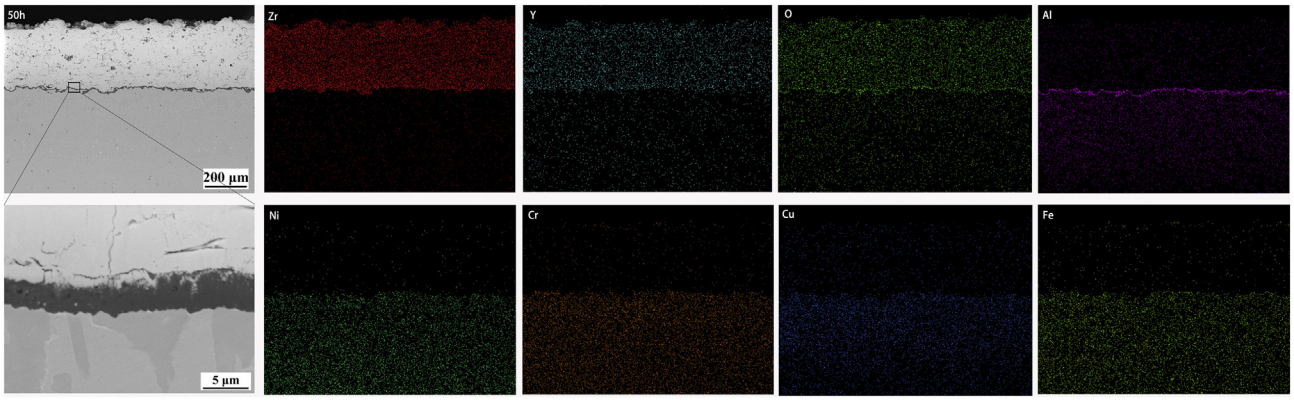

Fig. 9. The cross-section and EDS map scanning after isothermal oxidation at 1100 °C for 50 h when CuAlNiCrFe is used as the bond coat of TBC.

seen from the partial enlarged view in Fig. 9 that the alumina layer was tightly coupled with the ceramic layer and the metal bond coat, which fully demonstrates their further antioxidant potential.

4. Conclusions

(1) A high-speed laser cladding process was used to prepare a high-entropy alloy bond coat with metallurgical bonding with the Ni-based super-alloys substrate efficiently similar to the thermal spray process.
(2) CuAlNiCrFe high-entropy alloy bond coat deposited using high-speed laser cladding requires shorter pre-oxidation time, which shortens the initial oxidation stage and avoiding the formation of other oxides and spinel structures.
(3) A block-like structure of the bond coat instead of the thermal sprayed lamellar structure ensured a sufficient and continuous supply of Al element, which resulted in good high temperature oxidation resistance.
(4) The sluggish diffusion effect of high-entropy alloys ensured the slow growth rate of TGO and slow inter-diffusion between bond coat and substrate.
(5) The aluminum-containing high-entropy alloy bonding layer can maintain a simple solid solution structure with reduced Al content.

CRediT authorship contribution statement

Qing-Long Xu:Data curation, Writing - review & editing, Methodology.**Yu Zhang**:Investigation.**Sen-Hui Liu**:Visualization, Investigation.**Chang-Jiu Li**:Supervision.**Cheng-Xin Li**:Resources, Conceptualization.

Declaration of competing interest

The authors declare that they have no known competing financial interests or personal relationships that could have appeared to influence the work reported in this paper.

Acknowledgment

This work was financially supported by the National Key R&D Program of China (No.2018YFB2002000), National Natural Science Foundation of China (No.51761145108), and Key Technological Innovations Project of Shandong Province (2019JZZY010802).

References

[1] G. Meng, B. Zhang, H. Liu, G. Yang, T. Xu, C. Li, C. Li, Highly oxidation resistant and cost effective MCrAlY bond coats prepared by controlled atmosphere heat treatment, Surf. Coat. Technol. 347 (2018) 54–65, https://doi.org/10.1016/j.surfcoat.2018.04.068.
[2] A.G. Evans, D.R. Mumm, J.W. Hutchinson, Mechanisms controlling the durability of

thermal barrier coatings, Prog. Mater. Sci. 46 (2001) 505–553. https://doi.org/https://doi.org/10.1016/s0079-6425(00)00020-7.
[3] M.J. Stiger, N.M. Yanar, R.W. Jackson, S.J. Laney, F.S. Pettit, G.H. Meier, A.S. Gandhi, C.G. Levi, Development of intermixed zones of alumina/zirconia in thermal barrier coating systems, Metall. Mater. Trans. A. 38 (2007) 848–857. https://doi.org/https://doi.org/10.1007/s11661-007-9117-6.
[4] J. Toscano, R. Va, A. Gil, M. Subanovic, D. Naumenko, Parameters affecting TGO growth and adherence on MCrAlY-bond coats for TBC's, Surf. Coat. Technol. 201 (2006) 3906–3910, https://doi.org/10.1016/j.surfcoat.2006.07.247.
[5] H. Gaytor, B. Sc, E.P. D, High temperature alloys for gas turbines, Aircr. Eng. Aerosp. Technol. 47 (1975) 14–20, https://doi.org/10.1108/eb035213.
[6] D.M. Nissley, Thermal barrier coating life modeling in aircraft gas turbine engines, J. Therm. Spray Technol. 6 (1997) 91–98, https://doi.org/10.1007/BF02646317.
[7] V. Teixeira, M. Andritschky, W. Fischer, H.P. Buchkremer, D. Sto, Effects of deposition temperature and thermal cycling on residual stress state in zirconia-based thermal barrier coatings, Surf. Coatings Technol. 121 (1999) 103–111, https://doi.org/10.1016/s0257-8972(99)00341-2.
[8] W.R. Chen, X. Wu, B.R. Marple, D.R. Nagy, P.C. Patnaik, TGO growth behaviour in TBCs with APS and HVOF bond coats, Surf. Coatings Technol. 202 (2008) 2677–2683, https://doi.org/10.1016/j.surfcoat.2007.09.042.
[9] J.A. Haynes, M.K. Ferber, W.D. Porter, Thermal cycling behavior of plasma-sprayed thermal barrier coatings with various MCrAlX bond coats, J. Therm. Spray Technol. 9 (2000) 38–48, https://doi.org/10.1361/105996300770350041.
[10] R. Chen, X. Gong, Y. Wang, G. Qin, N. Zhang, Y. Su, H. Ding, J. Guo, H. Fu, Microstructure and oxidation behaviour of plasma-sprayed NiCoCrAlY coatings with and without Ta on Ti44Al6Nb1Cr alloys, Corros. Sci. 136 (2018) 244–254, https://doi.org/10.1016/j.corsci.2018.03.008.
[11] B. Zhang, G. Yang, C. Li, C. Li, Applied surface science non-parabolic isothermal oxidation kinetics of low pressure plasma sprayed MCrAlY bond coat, Appl. Surf. Sci. 406 (2017) 99–109, https://doi.org/10.1016/j.apsusc.2017.02.123.
[12] B. Zhang, G. Meng, G. Yang, C. Li, C. Li, Applied surface science dependence of scale thickness on the breaking behavior of the initial oxide on plasma spray bond coat surface during vacuum, Appl. Surf. Sci. 397 (2017) 125–132, https://doi.org/10.1016/j.apsusc.2016.11.140.
[13] J. Wang, M. Chen, Y. Cheng, L. Yang, Z. Bao, L. Liu, S. Zhu, F. Wang, Hot corrosion of arc ion plating NiCrAlY and sputtered nanocrystalline coatings on a nickel-based single-crystal superalloy, Corros. Sci. 123 (2017) 27–39, https://doi.org/10.1016/j.corsci.2017.04.004.
[14] A. Cahit, Turk Abdullah, Isothermal oxidation behavior and kinetics of thermal barrier coatings produced by cold gas dynamic spray technique, Surf. Coat. Technol. 318 (2017) 72–81, https://doi.org/10.1016/j.surfcoat.2016.12.021.
[15] M.J. Lance, J.A. Haynes, B.A. Pint, Performance of vacuum plasma spray and HVOF bond coatings at 900˚and 1100˚C, Surf. Coat. Technol. 337 (2018) 136–140, https://doi.org/10.1016/j.surfcoat.2017.12.062.
[16] G. Meng, H. Liu, M. Liu, T. Xu, G. Yang, C. Li, C. Li, Highly oxidation resistant MCrAlY bond coats prepared by heat treatment under low oxygen content, Surf. Coat. Technol. 368 (2019) 192–201, https://doi.org/10.1016/j.surfcoat.2019.04.046.
[17] M. Karadge, X. Zhao, M. Preuss, P. Xiao, Microtexture of the thermally grown alumina in commercial thermal barrier coatings, Scr. Mater. 54 (2006) 639–644, https://doi.org/10.1016/j.scriptamat.2005.10.043.
[18] J. Yeh, Alloy design strategies and future trends in high-entropy alloys, J. Miner. Met. Mater. Soc. 65 (2013) 1759–1771, https://doi.org/10.1007/s11837-013-0761-6.
[19] C. Tung, J. Yeh, T. Shun, S. Chen, Y. Huang, H. Chen, On the elemental effect of AlCoCrCuFeNi high-entropy alloy system, Mater. Lett. 61 (2007) 1–5, https://doi.org/10.1016/j.matlet.2006.03.140.
[20] W. Kai, W.L. Jang, R.T. Huang, C.C. Lee, H.H. Hsieh, C.F. Du, Air oxidation of FeCoNi-base equi-molar alloys at 800–1000˚C, Oxid. Met. 63 (2005) 169–192, https://doi.org/10.1007/s11085-004-3198-z.
[21] T.M. Butler, J.P. Alfano, R.L. Martens, M.L. Weaver, High-temperature oxidation behavior of Al-co-Cr-Ni-(Fe or Si) multicomponent high-entropy alloys, J. Miner. Met. Mater. Soc. 16 (2015) 246–259, https://doi.org/10.1007/s11837-014-1185-7.
[22] M. Jadhav, S. Singh, M. Srivastava, G.S.V. Kumar, An investigation on high entropy alloy for bond coat application in thermal barrier coating system, J. Alloys Compd. 783 (2019) 662–673, https://doi.org/10.1016/j.jallcom.2018.12.361.
[23] A. Anupam, S. Kumar, N.M. Chavan, B.S. Murty, R.S. Kottada, First report on cold-sprayed AlCoCrFeNi high-entropy alloy and its isothermal oxidation, J. Mater. Res. 38 (2019) 1–11, https://doi.org/10.1557/jmr.2019.38.
[24] Z. Liu, K.C. Chan, L. Liu, S.F. Guo, Bioactive calcium titanate coatings on a Zr-based bulk metallic glass by laser cladding, Mater. Lett. 82 (2012) 67–70, https://doi.org/10.1016/j.matlet.2012.05.022.
[25] Z. Xiaowei, L.I.U. Hongxi, W. Chuanqi, Z. Weihua, J. Yehua, Microstructure and high temperature oxidation resistance of TiN/Ti3Al intermetallic composite coatings on Ti6Al4V alloy by laser cladding, Proc. SPIE 7843 (2010) 1–10, https://doi.org/10.1117/12.870732.
[26] A. You, M.A.Y. Be, I. In, Investigations on ultra-high-speed laser material deposition as alternative for hard chrome plating and thermal spraying, J. Laser Appl. 28 (2016) 022501, https://doi.org/10.2351/1.4943910.
[27] B. Ruiz-yi, J.K. Bunn, D.M. Stasak, A. Mehta, M. Besser, M.J. Kramer, I. Takeuchi, J. Hattrick-simpers, The different roles of entropy and solubility in high entropy alloy stability the different roles of entropy and solubility in high entropy alloy stability, ACS Comb. Sci. (2016), https://doi.org/10.1021/acscombsci.6b00077.
[28] Y.L. Wang, Isothermal oxidation behavior of the directionally solidified Ni-based superalloy DZ951 AT 900, 1000 and 1100˚C, Int. J. Mod. Phys. B. 20 (2006) 3587–3592, https://doi.org/10.1142/S0217979206040039.
[29] M. Matsumoto, T. Kato, K. Hayakawa, N. Yamaguchi, S. Kitaoka, H. Matsubara, The effect of pre-oxidation atmosphere on the durability of EB-PVD thermal barrier coatings with CoNiCrAlY bond coats, Surf. Coat. Technol. 202 (2008) 2743–2748, https://doi.org/10.1016/j.surfcoat.2007.10.001.
[30] Y. Han, Z. Zhu, B. Zhang, Y. Chu, Y. Zhang, J. Fan, Effects of process parameters of vacuum pre-oxidation on the microstructural evolution of CoCrAlY coating deposited by HVOF, J. Alloys Compd. (2017), https://doi.org/10.1016/j.jallcom.2017.11.165.
[31] A. Hesnawi, H. Li, Z. Zhou, S. Gong, H. Xu, Effect of surface condition during pre-oxidation treatment on isothermal oxidation behavior of MCrAlY bond coat prepared by EB-PVD, Surf. Coat. Technol. 201 (2007) 6793–6796, https://doi.org/10.1016/j.surfcoat.2006.09.076.
[32] G. Meng, B. Zhang, H. Liu, G. Yang, T. Xu, C. Li, C. Li, Vacuum heat treatment mechanisms promoting the adhesion strength of thermally sprayed metallic coatings, Surf. Coat. Technol. 344 (2018) 102–110, https://doi.org/10.1016/j.surfcoat.2018.03.010.
[33] M. Matsumoto, K. Hayakawa, S. Kitaoka, H. Matsubara, H. Takayama, Y. Kagiya, Y. Sugita, The Effect of Preoxidation Atmosphere on Oxidation Behavior and Thermal Cycle Life of Thermal Barrier Coatings, 441 (2006), pp. 119–125, https://doi.org/10.1016/j.msea.2006.08.099.
[34] F. Morin, G. Beranger, P. Lacombe, Limits of application for Wagner's oxidation theory, Oxid. Met. 4 (1972) 51–62, https://doi.org/10.1007/BF00612507.
[35] M. Benegra, A.L.B. Santana, O. Maranho, G. Pintaude, Effect of heat treatment on wear resistance of nickel aluminide coatings deposited by HVOF and PTA, J. Therm. Spray Technol. 24 (2015) 1111–1116, https://doi.org/10.1007/s11666-015-0266-7.
[36] O. Maranho, D. Rodrigues, M.B. Jr, A. Sinatora, Mass loss and wear mechanisms of HVOF-sprayed multi-component white cast iron coatings, Wear 274–275 (2012) 162–167, https://doi.org/10.1016/j.wear.2011.08.024.
[37] M.S. Doolabi, B. Ghasemi, S.K. Sadrnezhaad, A. Habibolahzadeh, K. Jafarzadeh, Evaluation and selection of optimal oxygen/fuel ratio for best mechanical properties, oxidation resistance and microstructure of HVOF NiCoCrAlY coatings using AHP–VIKOR method, Oxid. Met. 89 (2018) 429–451, https://doi.org/10.1007/s11085-017-9797-2.
[38] Y.F. Ye, Q. Wang, J. Lu, C.T. Liu, Y. Yang, High-entropy alloy: challenges and prospects, Mater. Today 19 (2016) 349–362, https://doi.org/10.1016/j.mattod.2015.11.026.
[39] C. Li, G. Yang, C. Li, Development of particle Interface bonding in thermal spray coatings: a review, J. Therm. Spray Technol. 22 (2013) 192–206, https://doi.org/10.1007/s11666-012-9864-9.
[40] A. Weisenburger, G. Rizzi, A. Scrivani, G. Mueller, J.R. Nicholls, Pulsed electron beam treatment of MCrAlY bondcoats for EB-PVD TBC systems part 1 of 2: coating production, Surf. Coat. Technol. 202 (2007) 704–708, https://doi.org/10.1016/j.surfcoat.2007.07.022.
[41] J.A. Nesbitt, R.W. Heckel, Interdiffusion in Ni-rich, Ni-Cr-AI alloys at 1100 and 1200˚C : part II. Diffusion coefficients and predicted concentration profiles, Metall. Trans. A. 18A (1987) 2075–2086, https://doi.org/10.1007/BF02647079.
[42] S.R. Levine, Reaction diffusion in the NiCrAl and CoCrAl systems, Metall. Trans. A. 9 (1978) 1237–1250, https://doi.org/10.1007/BF02652247.
[43] V. Verma, A. Tripathi, K.N. Kulkarni, On interdiffusion in FeNiCoCrMn high entropy alloy, J. Phase Equilibria Diffus. 38 (2017) 445–456, https://doi.org/10.1007/s11669-017-0579-y.
[44] K. Tsai, M. Tsai, J. Yeh, Sluggish diffusion in Co–Cr–Fe–Mn–Ni high-entropy alloys, Acta Mater. 61 (2013) 4887–4897, https://doi.org/10.1016/j.actamat.2013.04.058.
[45] J. Da, Interdiffusion in the FCC-structured Al-Co-Cr-Fe-Ni high entropy alloys: experimental studies and numerical simulations, J. Alloys Compd. 674 (2016) 455–462, https://doi.org/10.1016/j.jallcom.2016.03.046.
[46] F.A. Golightly, F.H. Stott, G.C. Wood, The influence of yttrium additions on the oxide- scale adhesion to an iron-chromium-aluminum alloy, Oxid. Met. 10 (1976) 163–187, https://doi.org/10.1007/bf00612158.
[47] D.G. Lees, On the reasons for the effects of dispersions of stable oxides and additions of reactive elements on the adhesion and growth-mechanisms of chromia and alumina scales the "sulfur effect,", Oxid. Met. 27 (1987) 75–81, https://doi.org/10.1007/BF00656731.
[48] S. Darzens, D.R. Mumm, D.R. Clarke, A.G. Evans, Observations and analysis of the influence of phase transformations on the instability of the thermally grown oxide in a thermal barrier system, Metall. Mater. Trans. A. 34 (2003) 511–522, https://doi.org/10.1007/s11661-003-0087-z.
[49] D.R. Mumm, A.G. Evans, I.T. Spitsberg, Characterization of a cyclic displacement instability for a thermally grown oxide in a thermal barrier system, Acta Mater. 49 (2001) 2329–2340, https://doi.org/10.1016/s1359-6454(01)00071-4.
[50] L. Cen, W.Y. Qin, Q.M. Yu, On the role of TGO growth in the interface undulation in MCrAlY coating system upon thermal cycling, Ceram. Int. 45 (2019) 22802–22812, https://doi.org/10.1016/j.ceramint.2019.07.322.
[51] M.Y. He, A.G. Evans, J.W. Hutchinson, The ratcheting of compressed thermally grown thin films on ductile substrates, Acta Mater. 48 (2000) 2593–2601, https://doi.org/10.1016/s1359-6454(00)00053-7.
[52] J. Zhong, J. Liu, X. Zhou, S. Li, M. Yu, Z. Xu, Thermal cyclic oxidation and interdiffusion of NiCoCrAlYHf coating on a Ni-based single crystal superalloy, J. Alloys Compd. 657 (2016) 616–625, https://doi.org/10.1016/j.jallcom.2015.10.148.
[53] W. Wang, W. Wang, S. Wang, Y. Tsai, C. Lai, J. Yeh, Intermetallics effects of Al addition on the microstructure and mechanical property of Alx CoCrFeNi high-entropy alloys, Intermetallics 26 (2012) 44–51, https://doi.org/10.1016/j.intermet.2012.03.005.
[54] S. Laxman, B. Franke, B.W. Kempshall, Y.H. Sohn, L.A. Giannuzzi, K.S. Murphy,

Phase transformations of thermally grown oxide on (Ni,Pt)Al bondcoat during electron beam physical vapor deposition and subsequent oxidation, Surf. Coatings Technol 178 (2004) 121–130, https://doi.org/10.1016/j.surfcoat.2003.08.072.
[55] X. Liu, T. Wang, C. Li, Z. Zheng, Q. Li, Microstructural evolution and growth kinetics of thermally grown oxides in plasma sprayed thermal barrier coatings, Prog. Nat. Sci. Mater. Int. 26 (2016) 103–111, https://doi.org/10.1016/j.pnsc.2016.01.004.
[56] M. Saremi, A. Afrasiabi, A. Kobayashi, Microstructural analysis of YSZ and YSZ/Al2O3 plasma sprayed thermal barrier coatings after high temperature oxidation, Surf. Coatings Technol. 202 (2008) 3233–3238, https://doi.org/10.1016/j.surfcoat.2007.11.029.
[57] A.G. Evans, On the role of imperfections in the failure of a thermal barrier coating made by electron beam deposition, Acta Mater. 48 (2000) 1815–1827, https://doi.org/10.1016/s1359-6454(99)00473-5.
[58] K.M. Doleker, A.C. Karaoglanli, Comparison of oxidation behavior of YSZ and Gd2Zr2O7 thermal barrier coatings (TBCs), Surf. Coatings Technol. J. 318 (2017) 198–207, https://doi.org/10.1016/j.surfcoat.2016.12.078.
[59] H. Chen, A. Rushworth, Effects of oxide stringers on the β-phase depletion behaviour in thermally sprayed CoNiCrAlY coatings during isothermal oxidation, J. Mater. Sci. Technol. 45 (2020) 108–116, https://doi.org/10.1016/j.jmst.2019.11.018.
[60] M. Watanabe, D.R. Mumm, S. Chiras, A.G. Evans, Measurement of the residual stress in a Pt–aluminide bond coat, Scr. Mater. 46 (2002) 67–70, https://doi.org/10.1016/s1359-6462(01)01198-8.
[61] A. Kumar, N. Roy, A. Kar, A. Kumar, S. Chandra, G. Das, J. Kumar, D. Kumar, B. Venkataraman, S.V. Joshi, Mechanical property and characterization of a NiCoCrAlY type metallic bond coat used in turbine blade, Mater. Sci. Eng. A 505 (2009) 96–104, https://doi.org/10.1016/j.msea.2008.11.066.